First Observations of G-Band Radar Doppler Spectra

Geophysical Research Letters

RESEARCH LETTER
10.1029/2021GL096475

First Observations of G-Band Radar Doppler Spectra

Benjamin M. Courtier[1], Alessandro Battaglia[1,2,3], Peter G. Huggard[4], Chris Westbrook[5], Kamil Mroz[1,3], Ranvir S. Dhillon[1], Christopher J. Walden[4,6], Gareth Howells[4], Hui Wang[4], Brian N. Ellison[4], Richard Reeves[6,7], Duncan A. Robertson[8], and Richard J. Wylde[9]

[1]University of Leicester, Leicester, UK, [2]Politecnico of Torino, Turin, Italy, [3]National Centre for Earth Observation, Leicester, UK, [4]RAL Space, STFC Rutherford Appleton Laboratory, Didcot, UK, [5]Department of Meteorology, University of Reading, Reading, UK, [6]National Centre for Atmospheric Science, Leeds, UK, [7]STFC Chilbolton Observatory, Chilbolton, UK, [8]SUPA School of Physics and Astronomy, University of St Andrews, St Andrews, UK, [9]Thomas Keating Ltd., Billingshurst, UK

Abstract The first Doppler spectra ever acquired by an atmospheric radar at 200 GHz (G-band) are presented. The observations were taken during a light precipitation event in May (rain rates <2 mm hr^{-1}) at Chilbolton Observatory, UK, with coincident Ka-band and W-band Doppler radar measurements. The collected rain spectra agree with Mie theory predictions: at G-band they show significant reductions in the spectral power return—as compared to theoretical Rayleigh scattering—corresponding to high Doppler velocities (i.e., large raindrops) with the presence of multiple peaks and "Mie notches" in correspondence to the maxima and minima of the raindrop backscattering cross sections. The first two G-band Mie troughs correspond to smaller velocities/sizes than the first W-band Mie notch. These features offered by G-band radars pave the way toward applying, in rain, Mie notch vertical wind retrievals and multifrequency drop size distribution microphysical retrievals to smaller rain rates and smaller characteristic sizes than ever before.

Plain Language Summary The first Doppler velocity measurements ever acquired by an atmospheric radar at 200 GHz (in the so-called G-band) are presented. The observations were taken during a light precipitation event in May (rain rates <2 mm hr^{-1}) at the STFC Chilbolton Observatory, UK, with coincident measurements at 35 and 94 GHz. At high Doppler velocities (i.e., in correspondence to large raindrops) the collected G-band Doppler velocity spectra show significant non-Rayleigh effects, as expected from scattering Mie theory when the wavelength is much larger than the scattering target dimension. This is highlighted by the presence of multiple peaks and minima in the spectral power return and by a significant reduction of the spectral power at G-band compared to the other frequencies. The first two G-band minima both correspond to smaller velocities/sizes than the first W-band minimum, a direct consequence of the reduced wavelength of the G-band radar. These novel features observed by G-band radars pave the way toward applying, in rain, vertical wind retrievals and multifrequency drop size distribution retrievals to smaller rain rates and smaller characteristic drop sizes than ever before.

Key Points:

- The first Doppler spectra ever acquired by an atmospheric radar at 200 GHz (G-band) are presented
- The G-band spectra in rain show the presence of Mie notches, as expected from Mie scattering theory
- The G-band spectra pave the way toward applying vertical wind and multifrequency DSD retrievals at smaller rain rates than ever before

Correspondence to:
B. M. Courtier,
bmc19@leicester.ac.uk

Citation:
Courtier, B. M., Battaglia, A., Huggard, P. G., Westbrook, C., Mroz, K., Dhillon, R. S., et al. (2022). First observations of G-band radar Doppler spectra. *Geophysical Research Letters*, *49*, e2021GL096475. https://doi.org/10.1029/2021GL096475

Received 21 OCT 2021
Accepted 27 JAN 2022

Author Contributions:
Conceptualization: Alessandro Battaglia
Formal analysis: Benjamin M. Courtier, Alessandro Battaglia
Funding acquisition: Alessandro Battaglia
Investigation: Benjamin M. Courtier, Alessandro Battaglia
Methodology: Benjamin M. Courtier, Alessandro Battaglia, Peter G. Huggard, Chris Westbrook, Kamil Mroz, Ranvir S. Dhillon, Gareth Howells, Hui Wang, Brian N. Ellison, Duncan A. Robertson, Richard J. Wylde
Project Administration: Alessandro Battaglia, Chris Westbrook
Resources: Peter G. Huggard, Hui Wang, Brian N. Ellison, Richard Reeves, Duncan A. Robertson, Richard J. Wylde
Software: Benjamin M. Courtier, Alessandro Battaglia, Chris Westbrook, Kamil Mroz, Gareth Howells
Supervision: Alessandro Battaglia

1. Introduction

In the last three decades mm wavelength radars within the Ka-bands and W-bands have proved to be paramount tools for cloud and precipitation process studies (Kneifel & Moisseev, 2020; Ori et al., 2020) and long-term cloud monitoring (Kollias et al., 2020; Stein et al., 2015; Tridon, Battaglia & Watters, 2017). This success has been driven by their larger sensitivity to small droplets and ice crystals (Lhermitte, 1990), their superior spatial resolution, and their reduced susceptibility to Bragg scattering compared with centimeter-wavelength radars in the S, C, and X bands (Kollias et al., 2007), whereas their portability and compactness have made them suitable instruments to be deployed on ships (e.g., Protat et al., 2016), aircraft (e.g., Walker McLinden et al., 2021), and spacecraft. The latter application is demonstrated by the W-band CloudSat and the Ka-band GPM radars (Battaglia et al., 2020, and references therein). Synergistic measurements which combine multifrequency centimeter and millimeter wavelength radars (e.g., Chase et al., 2018; Neto et al., 2019), possibly including lidar and radiometer characterizations (e.g., Petäjä et al., 2016), underpin sophisticated quantitative retrievals of cloud and precipitation microphysics and dynamics (e.g., Delanoë & Hogan, 2008; Fielding et al., 2015; Battaglia et al., 2016; Mason et al., 2017, 2018; Mroz et al., 2021; Tridon et al., 2019; Oue et al., 2021) at many global locations (Illingworth et al., 2007; Kollias et al., 2020).

Writing – original draft: Benjamin M. Courtier
Writing – review & editing: Alessandro Battaglia, Peter G. Huggard, Chris Westbrook, Kamil Mroz, Ranvir S. Dhillon, Gareth Howells, Hui Wang, Brian N. Ellison, Duncan A. Robertson, Richard J. Wylde

More recently, breakthroughs in solid-state radar technology (in particular the development of high power Schottky diode-based frequency multiplied sources and solid-state power amplifiers) have enabled the construction of radars in the next highest, useable frequency waveguide band, the G-band with frequencies between 140 and 220 GHz (IEEE, 2016). The first G-band meteorological radar was developed as a Differential Absorption Radar (DAR; Cooper et al., 2018), to measure the water vapor and humidity profiles in boundary layer clouds (Roy et al., 2018). The radar's measurements were validated against radiosondes and found to be in close agreement with the in situ measurements (Roy et al., 2020). Using the same radar, Lamer et al. (2020) presented the first multifrequency observations including a G-band radar, showing that the differential reflectivity of the Ka-G pairing was several decibels greater than that of the traditional Ka-W pairing. They also showed evidence for non-Rayleigh scattering in the G-band where the Ka-band and W-band signals were still experiencing Rayleigh scattering. The improved dynamic range in multifrequency reflectivity ratios enables microphysical retrievals for clouds and precipitation characterized by smaller particle size and/or equivalent water contents (Battaglia et al., 2014).

G-band radars also have the potential to improve on other methods of profiling boundary layer clouds. Current techniques involve lidars (O'Connor et al., 2005; Westbrook et al., 2010), which cannot see above the cloud base from the ground. To mitigate this, Fielding et al. (2015) used a combination of radar, lidar, and zenith radiances; however, this methodology cannot be used if precipitation is reaching the surface. G-band radars present an opportunity to bypass these restrictions and retrieve a better estimation of the Particle Size Distribution (PSD). Unfortunately, G-band radiation is subject to a strong frequency dependent attenuation by water vapor and other atmospheric gases. This is exacerbated at warmer temperatures, due to the higher atmospheric absolute humidity. This means that G-band radars are more useful in cooler, subtropical regions in the winter (Battaglia et al., 2014).

In this study, the first results from a new G-band radar are presented, including the first Doppler spectra measured by a G-band radar. The radars and other instruments used in this study are detailed in Section 2. The results are presented in Section 3 and finally conclusions are drawn in Section 4.

2. Radars and Operation

Chilbolton Observatory is located in the south of England (51°08′40″N, 1°26′19″W). The observatory routinely operates a Ka-band radar in support of long-term measurements by the National Centre for Atmospheric Science (NCAS), and provides tailored use to the research community of a W-band radar as part of the Atmospheric Measurement and Observation Facility (AMOF). The Observatory has been recently equipped with the G-band Radar for Cloud Evaluation (GRaCE).

GRaCE is a zenith looking solid-state pulsed Doppler radar, operating at a frequency of 199.5 GHz. This frequency is a three-way compromise between atmospheric transmission, which increases away from the absorption of the 183 GHz water vapor line, the increasing cost of generating the power to efficiently drive the frequency doubler, and the maximum permitted by the UK licensing authority, Ofcom, at 200 GHz. The transmit signal is derived from a low phase noise, Ka-band, dielectric resonator oscillator, the output of which is pulsed by a PIN diode switch and then amplified. The 33.25 GHz signal drives a frequency tripler, whose output is in turn power amplified and then frequency doubled to obtain an 80 mW output power transmit signal. The transmit pulse passes through a low loss, high isolation, quasi-optical duplexer to a single high gain, 65 dBi, 1 m aperture, reflector antenna system. The antenna beam is projected vertically upwards using a 45° plane mirror, the beam width is 0.11°.

GRaCE was operated in IQ recording mode and spectra were calculated from the raw IQ data using 512 FFT points and were then averaged over a period of 2 s (or 98 spectra). The Pulse Repetition Frequency (PRF) was 25 kHz, meaning the radar had a Nyquist velocity of ± 9.38 m s^{-1}. The range resolution was 60 m and the overall range was kept to just 6 km, due to the sensitivity of the radar (-5 dBZ at 1 km, averaged over 2 s) that did not allow for observations at higher altitudes (this will be improved in the future with improvements to the hardware).

The W-band radar is a zenith pointing pulsed Doppler radar operating at a frequency of 94 GHz with a 1,500 W transmitted peak power. It operates using twin 0.46 m antennas with a 0.5° beam width, the range resolution was 60 m and the minimum range is about 200 m. As in the case of GRaCE, the spectra for this radar were composed of 512 FFT points and were also averaged over 2 s (or 24 spectra) giving a sensitivity of -15 dBZ at a range of

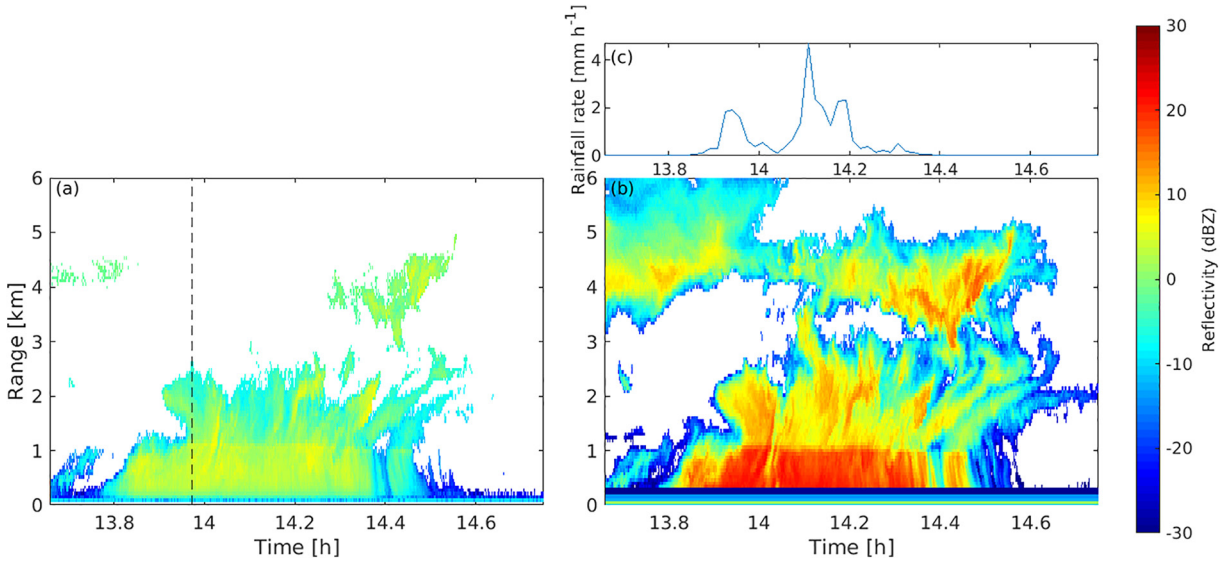

Figure 1. Radar reflectivity of (a) G-band Radar for Cloud Evaluation (GRaCE) and (b) the W-band radar on May 24, 2021. Panel (c) shows the rainfall rate during the time that observations were collected over. The reflectivity of GRaCE has been calibrated against simulated reflectivity derived from ground disdrometer observations and the reflectivity of the W-band cross calibrated against the 3 GHz radar at Chilbolton. Dashed line shows the time at which the spectrogram shown in Figure 2 was taken.

1 km. The PRF of this radar was 6,250 Hz and the Nyquist velocity was ±4.98 m s^{-1}, giving an unambiguous range of 24.0 km, much larger than that of GRaCE.

The Ka-band radar is a zenith pointing pulse Doppler radar operating at a frequency of 35 GHz with a 1,500 W transmitted peak power. It operates using a single 2.4 m antenna with 0.25° beam width, the range resolution was 60 m and the minimum range is about 250 m. The Ka-band radar was also used in IQ recording mode; the data were used to generate 512 FFT point spectra and averaged over 2 s (or 18 spectra), giving a sensitivity of −10 dBZ at a range of 1 km. The PRF of this radar was 5 kHz giving a Nyquist velocity of ±10.7 m s^{-1}, and an unambiguous range of 30.0 km.

Both the W-band and Ka-band radars have been calibrated to within 1.5 dB through comparison with the 3 GHz radar at Chilbolton. The 3 GHz radar has, in turn, been calibrated to better than 0.5 dB using the nonindependence of its dual-polarization parameters (Goddard et al., 1994).

The W-band and Ka-band radars were situated adjacent to one another, with the G-band radar 30 m away. Though efforts were made to ensure each radar was vertically pointing, small 0.4° and 0.15° pointing errors were found in the Ka-band and W-band radars, respectively. This is somewhat mitigated by the fact that the measurements presented here were taken at low altitudes and through a relatively homogeneous region of the cloud and precipitation.

To calibrate the measurements of GRaCE, the G-band reflectivity data were compared against reflectivity modeled from disdrometer observations 2 min subsequent to the GRaCE observations at the closest available range (300 m), similar to the approach followed by Lamer et al. (2020). The 2 min gap between the disdrometer based spectra and the GRaCE observations was to allow time for the drops to fall the 300 m from the nearest range gate to the disdrometer, two-way path integrated gaseous attenuation has also been taken in to account for the calibration.

3. Results and Discussion

GRaCE was used together with the W-band and Ka-band radars to collect observations of scattered showers on the May 24, 2021, in particular a shallow, precipitating cloud from a frontal system that passed over the radars between 13.45 UT and 14.45 UT (the event is shown in Figure 1). Observations from the W-band radar show the cloud had a depth of around 3 km with the melting layer at an altitude of about 1 km. The maximum reflectivities

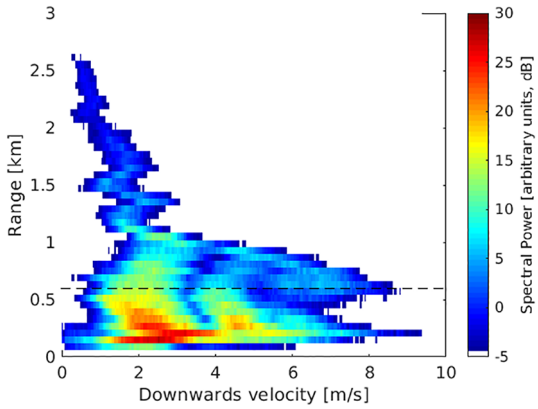

Figure 2. Spectrogram (stack of Doppler spectra with height) from G-band Radar for Cloud Evaluation (GRaCE) at 13.59 UT (marked in Figure 1a with a dashed line), positive velocities indicated downward motion. The dashed line shows the altitude of the spectrum presented in Figure 3.

of the precipitation were measured at 22.3 dBZ by the W-band radar, which is close to the maximum reflectivity that can be observed by a W-band radar (Hogan et al., 2003).

This cloud was deemed to be a good test of GRaCE due to the relatively shallow depth and light precipitation, compared to other precipitating cells on the day; it provides an excellent case to show the capabilities of GRaCE and the spectra produced by light rain.

The reflectivity shown in Figure 1a is, as expected, consistently lower than the reflectivity shown in Figure 1b, from the W-band radar. This is a combination of non-Rayleigh scattering and the effects of the increased attenuation experienced at G-band frequencies from both atmospheric gases and the hydrometeors themselves (Battaglia et al., 2020). The effect of increased attenuation is particularly obvious in the reflectivity returns above 3 km altitude at 14.10 UT, where the W-band radar measures signals greater than 0 dBZ, but the GRaCE reflectivity has been completely attenuated.

The spectra used for the rest of this study were taken at 13.59 UT (marked in Figure 1 with a dashed line) at which time the precipitation was relatively light and steady. The rain rate peaked at around 2 mm hr^{-1} a few minutes after the spectra were observed and the mass mean droplet diameter (D_m) remained steady at around 0.9 mm for a few minutes within the acquisition time of the spectra shown here. The reflectivity from the W-band radar shows that the cloud extends to an altitude of around 3 km at this time, with another thin ice cloud 2 km above that.

The spectra from GRaCE at 13.59 UT (Figure 2) feature a strong signal up to approximately 1.1 km, the expected height of the freezing level and then weaker signal up to an altitude of 2.5 km. These are the returns related to the liquid and ice regions of the cloud that are separated by a melting layer characterized by a strong vertical gradient in the range of Doppler velocities. Note that despite the signal being strongly attenuated by the rain and the potential liquid cloud layers, GRaCE has some capability in detecting the top of the ice portion of the low cloud. The radar returns in the liquid layer also show the characteristic appearance of Mie notches at velocities of around 3 and 5 m s^{-1}, though the second Mie notch is confined only to the layer between 0.3 and 1 km altitude, where larger drops are present (below 300 m near field effects prevent the detection of Mie notches). The differences between the observed velocities of the Mie notches and the theoretical Mie notches (calculated using T-matrix modeling of realistically shaped raindrops at various canting angles) at this frequency (3.2 m s^{-1} or 0.8 mm and 5.0 m s^{-1} or 1.5 mm for G-band and 5.9 m s^{-1} or 1.9 mm for W-band, as shown in Figure 3b) is a result of the vertical wind (Kollias et al., 2002). The locations of the Mie notches can also be affected by turbulent broadening

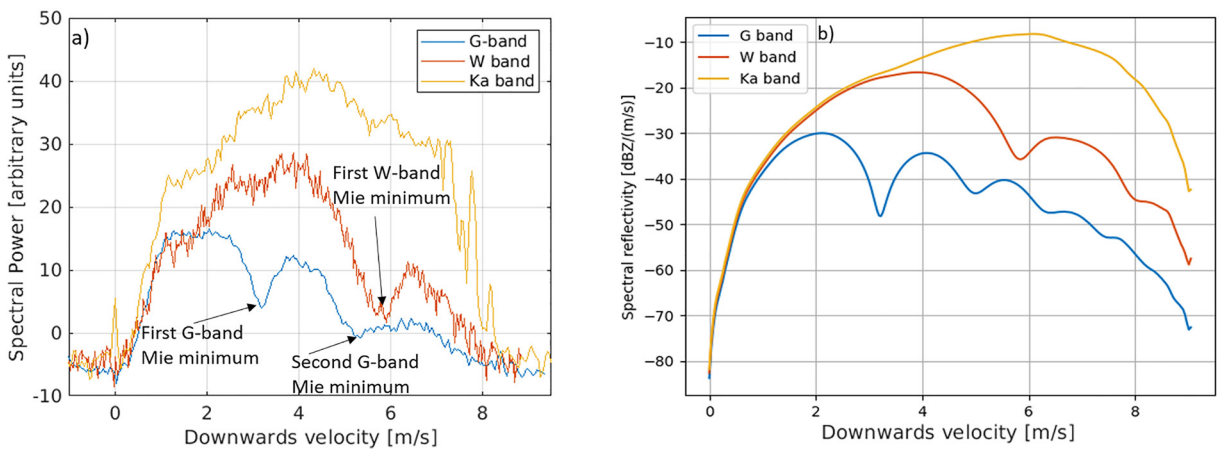

Figure 3. (a) Spectra from G-band Radar for Cloud Evaluation (GRaCE), the W-band and the Ka-band radars at 13.59 UT and 600 m altitude. The W-band data has been unfolded to give approximately the same maximum velocity as the G-band and Ka-band radars. The three spectra have been aligned to match the Rayleigh regions of the spectra, but have not been calibrated. (b) Theoretical spectra for an exponential Particle Size Distribution (PSD) with a D_m of 1 mm.

Table 1
The Difference of the Location of the Theoretical Mie Notches Due To Spectral Broadening From the Spectra in Figure 3b in m s^{-1}

	Turbulence		
Mie Notch	0.05 m^2 s^{-3}	0.1 m^2 s^{-3}	0.2 m^2 s^{-3}
G-band notch 1	0	0.01	0.04
G-band notch 2	0	0.02	0.08
W-band notch 1	0	0.02	0.08

of the spectra. This does not have a large impact on the location of the Mie notches until the turbulence reaches high values, as is shown in Table 1.

Figure 3a shows the spectra from GRaCE, the W-band radar and the Ka-band radar at 600 m altitude. In the spectral region with Doppler velocities between 0 and 0.5 m s^{-1} the three curves follow approximately the same evolution: this is the region corresponding to targets that backscatter in the Rayleigh regime for all three radar frequencies. The W-band and Ka-band maintain the same behavior in a wider region, as they remain in the Rayleigh regime for larger (and therefore faster falling) droplets.

In Figure 3a, it can be seen that the two Mie notches in the GRaCE spectrum occur at smaller Doppler velocities than the first and only minimum of the W-band spectrum. The theoretical velocity at which the Mie minima should occur for droplets falling in still air can be computed via Mie theory (Lhermitte, 1990), this is done here using the same method as Mróz et al. (2021): an example for an exponential PSD is shown in Figure 3b. These theoretical computations can be used in combination with the location of the observed minima to retrieve the vertical wind speed by using the method of Kollias et al. (2002). The lower vertical velocity of the Mie minima at 200 GHz as compared with 94 GHz allows for the retrieval of the vertical wind speed for smaller droplets with lower fall speeds, and correspondingly much lower rain rates, than would be possible using a W-band radar. It also gives a reduced level of uncertainty to the measurements as the individual estimates from the two Mie notches can be averaged to give a more reliable vertical wind measurement whereas the range of values can be used to give an estimate of the uncertainty.

The vertical wind retrieval results from GRaCE using this method are shown in Figure 4a. Here the Mie notches are detected automatically from smoothed spectra by allowing a maximum deviation from the theoretical values of 0.6 m s^{-1}; where two Mie notches are detected the average of the notches' velocities are used for the estimate of vertical wind. It can be seen that GRaCE detects at least one Mie notch (and therefore an estimate of the vertical wind speed) through a large portion of the precipitation event. In comparison, the W-band radar only measured a small number of vertical wind points between 14 UT and 14.30 UT (shown in Figure 4b).

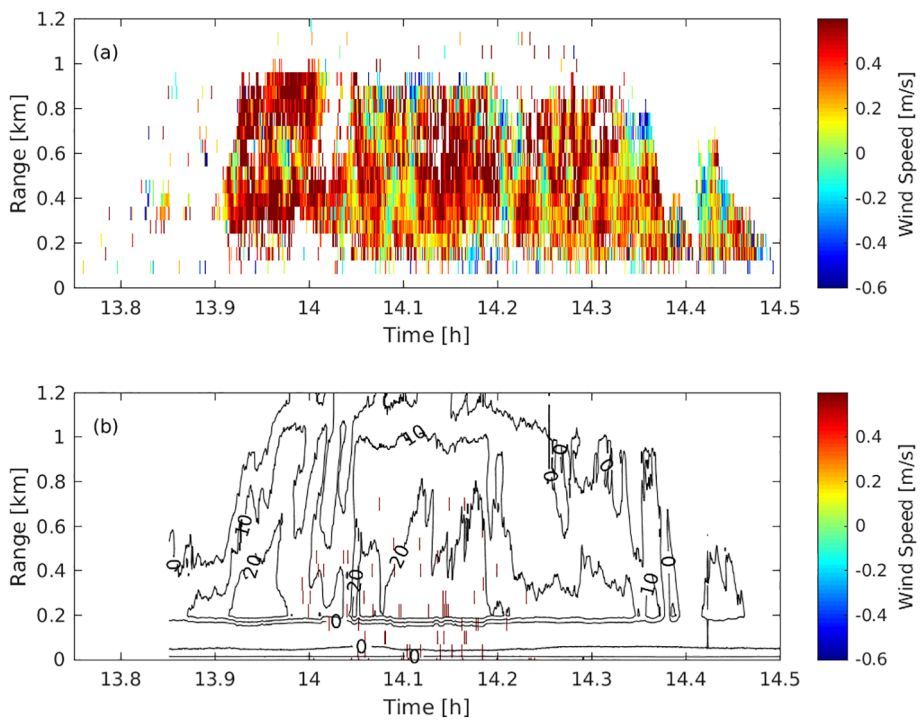

Figure 4. (a) Vertical wind speed from G-band Radar for Cloud Evaluation (GRaCE), using the Mie notch method of Kollias et al. (2002), as described in text. (b) Vertical wind speed from the W-band radar, also using the Mie notch method of Kollias et al. (2002). Overlaid contours in panel b show the radar reflectivity of the Ka-band radar.

The reduced spectral reflectivity compared to the W-band radar at small velocities (around 2 m s^{-1}) associated with non-Rayleigh effects paves the way toward the use of retrieval techniques at lower rain rates and enables the derivation of raindrop concentrations to lower drop sizes. Our results demonstrate the potential of a G-band system when used in parallel with conventional millimeter radars at Ka-bands and W-bands. For instance, when applying their optimal estimation retrieval technique to Ka-W-band dual frequency radar synthetic data observations, Tridon and Battaglia (2015) could not produce PSDs with a mass mean droplet diameter (D_m) below 1 mm because the Mie effects were too weak in both the W-band and Ka-band frequencies to allow for the correction of the vertical wind; this is mitigated with the use of G-band (potentially together with both the Ka-bands and W-bands, following the example of Mróz et al. (2021)). Further Tridon and Battaglia (2015) note that their optimal estimation method could be extended to the retrieval of light rain and drizzle by the use of G-band; the results shown here appear to corroborate that suggestion.

4. Conclusions

The ground-breaking 199.5 GHz GRaCE (G-band Radar for Cloud Evaluation), deployed at the UK's Chilbolton Observatory, has recorded the first G-band Doppler spectra from meteorological targets.

The radar was used to observe a light rain event, with rain rates lower than 2 mm hr^{-1}, on the May 24, 2021; the results featured spectra with a significant reduction in the spectral power return corresponding to high Doppler velocities (i.e., large raindrops). This is due to non-Rayleigh effects and, at longer ranges, due to attenuation, the non-Rayleigh effects are shown by the presence of multiple peaks and "Mie notches" in correspondence to the maxima and minima of the raindrop backscattering cross sections.

The first two Mie notches from GRaCE are both at lower velocities than the first Mie notch from the W-band radar, as expected from theory. This gives an increased sensitivity to vertical wind measurements, allowing the retrieval of vertical wind speed in lighter rain than with the use of W-band radar. At the GRaCE frequency, the onset of non-Rayleigh scattering occurs in correspondence to smaller particles than at the cloud radar frequencies currently operated. As a consequence, dual or triple-frequency techniques involving a G-band frequency have the potential to extend drop size distribution microphysical retrievals to smaller rain rates and smaller characteristic drop sizes. Future work will be devoted to developing rain microphysical retrievals to multifrequency (including the G-band) Doppler spectra by mimicking what has already been done with X-band, Ka-band, and W-band combinations (Tridon et al., 2013; Tridon, Battaglia, Luke, et al., 2017). In addition, the acquisition of G-band Doppler spectra in ice during the next Autumn and Winter (when the attenuation will have a less detrimental impact) will allow exploring ice scattering properties at unprecedented size parameters and therefore enable a better understanding of ice electromagnetic and scattering models (Kneifel et al., 2016, 2020; Stein et al., 2015).

Acknowledgments
The work done by B. M. Courtier, A. Battaglia, and C. D. Westbrook was funded by the UK NERC project GRACES (G-band RAdar for Cloud and prEcipitation Studies, Grant No. RP16G1219). The instrument development work by D. A. Robertson, R. J. Wylde, H. Wang, G. Howells, B. N. Ellison, and P. G. Huggard was funded by the UK-CEOI project GRaCE. The work by K. Mroz was performed at the University of Leicester under Grant No. RP1890005 with the National Centre for Earth Observation. C. D. Westbrook's contribution was also supported by a Research Endowment Trust Fund award from the University of Reading. Operation of the Chilbolton Ka-band and W-band radars was funded as part of NERC National Capability. We would like to thank Karina McCusker and Emal Rumi for coordinating the collection of 35 and 94 GHz radar data as part of the NERC PICASSO project, Grant No. NE/P012426/1.

Data Availability Statement

Data are available in the Zenodo online repository (Courtier et al., 2021) at https://zenodo.org/record/5548069.

References

Battaglia, A., Kollias, P., Dhillon, R., Roy, R., Tanelli, S., Lamer, K., et al. (2020). Spaceborne cloud and precipitation radars: Status, challenges, and ways forward. *Reviews of Geophysics*, *58*, e2019RG000686. https://doi.org/10.1029/2019RG000686

Battaglia, A., Mroz, K., Lang, T., Tridon, F., Tanelli, S., Tian, L., et al. (2016). Using a multiwavelength suite of microwave instruments to investigate the microphysical structure of deep convective cores. *Journal of Geophysical Research*, *121*, 9356–9381. https://doi.org/10.1002/2016JD025269

Battaglia, A., Westbrook, C. D., Kneifel, S., Kollias, P., Humpage, N., Löhnert, U., et al. (2014). G band atmospheric radars: New frontiers in cloud physics. *Atmospheric Measurement Techniques*, *7*(6), 1527–1546. https://doi.org/10.5194/amt-7-1527-2014

Chase, R. J., Finlon, J. A., Borque, P., McFarquhar, G. M., Nesbitt, S. W., Tanelli, S., et al. (2018). Evaluation of triple-frequency radar retrieval of snowfall properties using coincident airborne in situ observations during OLYMPEX. *Geophysical Research Letters*, *45*, 5752–5760. https://doi.org/10.1029/2018GL077997

Cooper, K. B., Rodriguez Monje, R., Millan, L., Lebsock, M., Tanelli, S., Siles, J. V., et al. (2018). Atmospheric humidity sounding using differential absorption radar near 183 GHz. *IEEE Geoscience and Remote Sensing Letters*, *15*(2), 163–167. https://doi.org/10.1109/LGRS.2017.2776078

Courtier, B., Westbrook, C., Battlaglia, A., Huggard, P., Walden, C., McCusker, K., & Rumi, E. (2021). Triple-frequency (Ka-, W- and G-band) radar observations of a light precipitation event. [Data set] Zenodo. https://doi.org/10.5281/zenodo.5548069

Delanoë, J. M., & Hogan, R. J. (2008). A variational scheme for retrieving ice cloud properties from combined radar, lidar, and infrared radiometer. *Journal of Geophysical Research*, *113*, D07204. https://doi.org/10.1029/2007JD009000

Fielding, M. D., Chiu, J. C., Hogan, R. J., Feingold, G., Eloranta, E., O'Connor, E. J., et al. (2015). Joint retrievals of cloud and drizzle in marine boundary layer clouds using ground-based radar, lidar and zenith radiances. *Atmospheric Measurement Techniques*, *8*(7), 2663–2683. https://doi.org/10.5194/amt-8-2663-2015

Goddard, J., Thurai, M., & Eastment, J. (1994). The Chilbolton advanced meteorological radar: A tool for multidisciplinary atmospheric research. *Electronics & Communication Engineering Journal*, *6*(2), 77–86. https://doi.org/10.1049/ecej:19940205

Hogan, R. J., Bouniol, D., Ladd, D. N., O'connor, E. J., & Illingworth, A. J. (2003). Absolute calibration of 94/95-GHz radars using rain. *Journal of Atmospheric and Oceanic Technology*, *20*, 572–580. https://doi.org/10.1175/1520-0426(2003)20<572:ACOGRU>2.0.CO;2

IEEE. (2016). *IEEE standard for rectangular metallic waveguides and their interfaces for frequencies of 110 GHz and above—Part 2: Waveguide interfaces* (Tech. Rep.). IEEE. https://doi.org/10.1109/IEEESTD.2016.7564020

Illingworth, A. J., Hogan, R. J., O'Connor, E. J., Bouniol, D., Brooks, M. E., Delanoë, J., et al. (2007). Cloudnet: Continuous evaluation of cloud profiles in seven operational models using ground-based observations. *Bulletin of the American Meteorological Society*, *88*(6), 883–898. https://doi.org/10.1175/BAMS-88-6-883

Kneifel, S., Kollias, P., Battaglia, A., Leinonen, J., Maahn, M., Kalesse, H., et al. (2016). First observations of triple-frequency radar Doppler spectra in snowfall: Interpretation and applications. *Geophysical Research Letters*, *43*, 2225–2233. https://doi.org/10.1002/2015GL067618

Kneifel, S., Leinonen, J., Tyynela, J., Ori, D., & Battaglia, A. (2020). Scattering of hydrometeors. In V. Levizzani (Ed.), *Satellite precipitation measurement* (Vol. 1). Springer. https://doi.org/10.1007/978-3-030-24568-9_15

Kneifel, S., & Moisseev, D. (2020). Long-term statistics of riming in nonconvective clouds derived from ground-based Doppler cloud radar observations. *Journal of the Atmospheric Sciences*, *77*(10), 3495–3508. https://doi.org/10.1175/JAS-D-20-0007.1

Kollias, P., Albrecht, B. A., & Marks, F. (2002). WHY MIE? Accurate observations of vertical air velocities and raindrops using a cloud radar scattering of microwave radiation by large particles-Mie scattering-makes possible an innovative method for observing precipitation using 94-Ghz Doppler radar. *Bulletin of the American Meteorological Society*, *83*(10), 1471–1484. https://doi.org/10.1175/BAMS-83-10-1471

Kollias, P., Bharadwaj, N., Clothiaux, E. E., Lamer, K., Oue, M., Hardin, J., et al. (2020). The ARM radar network: At the leading edge of cloud and precipitation observations. *Bulletin of the American Meteorological Society*, *101*(5), E588–E660. https://doi.org/10.1175/BAMS-D-18-0288.1

Kollias, P., Clothiaux, E. E., Miller, M. A., Albrecht, B. A., Stephens, G. L., & Ackerman, T. P. (2007). Millimeter-wavelength radars new frontier in atmospheric cloud and precipitation research. *Bulletin of the American Meteorological Society*, *88*, 1608–1624. https://doi.org/10.1175/bams-88-10-1608

Lamer, K., Oue, M., Battaglia, A., Roy, R., Cooper, K., Dhillon, R., et al. (2020). First light multi-frequency observations with a G-band radar. *Atmospheric Measurement Techniques Discussions*, 1–25. https://doi.org/10.5194/amt-2020-493

Lhermitte, R. (1990). Attenuation and scattering of millimeter wavelength radiation by clouds and precipitation. *Journal of Atmospheric and Oceanic Technology*, *7*, 464–479. https://doi.org/10.1175/1520-0426(1990)007<0464:AASOMW>2.0.CO;2

Mason, S. L., Chiu, C. J., Hogan, R. J., Moisseev, D., & Kneifel, S. (2018). Retrievals of riming and snow density from vertically pointing Doppler radars. *Journal of Geophysical Research: Atmospheres*, *123*, 807–813. https://doi.org/10.1029/2018JD028603

Mason, S. L., Chiu, J. C., Hogan, R. J., & Tian, L. (2017). Improved rain rate and drop size retrievals from airborne Doppler radar. *Atmospheric Chemistry and Physics*, *17*(18), 11567–11589. https://doi.org/10.5194/acp-17-11567-2017

Mróz, K., Battaglia, A., Kneifel, S., Von Terzi, L., Karrer, M., & Ori, D. (2021). Linking rain into ice microphysics across the melting layer in stratiform rain: A closure study. *Atmospheric Measurement Techniques*, *14*(1), 511–529. https://doi.org/10.5194/amt-14-511-2021

Mroz, K., Battaglia, A., Nguyen, C., Heymsfield, A., Protat, A., & Wolde, M. (2021). Triple frequency radar retrieval of microphysical properties of snow. *Atmospheric Measurement Techniques Discussions*, *14*, 7243–7254. https://doi.org/10.5194/amt-14-7243-2021

Neto, J. D., Kneifel, S., Ori, D., Trömel, S., Handwerker, J., Bohn, B., et al. (2019). The TRIple-frequency and Polarimetric radar Experiment for improving process observations of winter precipitation. *Earth System Science Data*, *11*(2), 845–863. https://doi.org/10.5194/essd-11-845-2019

O'Connor, E. J., Hogan, R. J., & Illingworth, A. J. (2005). Retrieving Stratocumulus drizzle parameters using Doppler radar and lidar. *Journal of Applied Meteorology and Climatology*, *44*(1), 14–27.

Ori, D., Schemann, V., Karrer, M., Dias Neto, J., von Terzi, L., Seifert, A., et al. (2020). Evaluation of ice particle growth in ICON using statistics of multi-frequency Doppler cloud radar observations. *Quarterly Journal of the Royal Meteorological Society*, *146*(733), 3830–3849. https://doi.org/10.1002/qj.3875

Oue, M., Kollias, P., Matrosov, S. Y., Battaglia, A., & Ryzhkov, A. V. (2021). Analysis of the microphysical properties of snowfall using scanning polarimetric and vertically pointing multi-frequency Doppler radars. *Atmospheric Measurement Techniques*, *14*(7), 4893–4913. https://doi.org/10.5194/amt-14-4893-2021

Petäjä, T., O'Connor, E. J., Moisseev, D., Sinclair, V. A., Manninen, A. J., Väänänen, R., et al. (2016). A field campaign to elucidate the impact of biogenic aerosols on clouds and climate. *Bulletin of the American Meteorological Society*, *97*(10), 1909–1928. https://doi.org/10.1175/BAMS-D-14-00199.1

Protat, A., Delanoë, J., Strapp, J. W., Fontaine, E., Leroy, D., Schwarzenboeck, A., et al. (2016). The measured relationship between ice water content and cloud radar reflectivity in tropical convective clouds. *Journal of Applied Meteorology and Climatology*, *55*, 1707–1729. https://doi.org/10.1175/JAMC-D-15-0248.1

Roy, R. J., Lebsock, M., Millán, L., & Cooper, K. B. (2020). Validation of a G-band differential absorption cloud radar for humidity remote sensing. *Journal of Atmospheric and Oceanic Technology*, *37*(6), 1085–1102. https://doi.org/10.1175/JTECH-D-19-0122.1

Roy, R. J., Lebsock, M., Millán, L., Dengler, R., Rodriguez Monje, R., Siles, J. V., et al. (2018). Boundary-layer water vapor profiling using differential absorption radar. *Atmospheric Measurement Techniques*, *11*(12), 6511–6523. https://doi.org/10.5194/amt-11-6511-2018

Stein, T. H., Westbrook, C. D., & Nicol, J. C. (2015). Fractal geometry of aggregate snowflakes revealed by triple-wavelength radar measurements. *Geophysical Research Letters*, *42*, 176–183. https://doi.org/10.1002/2014GL062170

Tridon, F., & Battaglia, A. (2015). Dual-frequency radar Doppler spectral retrieval of rain drop size distributions and entangled dynamics variables. *Journal of Geophysical Research: Atmospehres*, *120*, 5585–5601. https://doi.org/10.1002/2014JD023023

Tridon, F., Battaglia, A., Chase, R. J., Turk, F. J., Leinonen, J., Kneifel, S., et al. (2019). The microphysics of stratiform precipitation during OLYMPEX: Compatibility between triple-frequency radar and airborne in situ observations. *Journal of Geophysical Research: Atmospheres*, *124*, 8764–8792. https://doi.org/10.1029/2018JD029858

Tridon, F., Battaglia, A., & Kollias, P. (2013). Disentangling Mie and attenuation effects in rain using a Ka-W dual-wavelength Doppler spectral ratio technique. *Geophysical Research Letters*, *40*, 5548–5552. https://doi.org/10.1002/2013GL057454

Tridon, F., Battaglia, A., Luke, E., & Kollias, P. (2017). Rain retrieval from dual-frequency radar Doppler spectra: Validation and potential for a midlatitude precipitating case-study. *Quarterly Journal of the Royal Meteorological Society*, *143*(704), 1364–1380. https://doi.org/10.1002/qj.3010

Tridon, F., Battaglia, A., & Watters, D. (2017). Evaporation in action sensed by multiwavelength Doppler radars. *Journal of Geophysical Research: Atmospheres*, *122*, 9379–9390. https://doi.org/10.1002/2016JD025998

Walker McLinden, M. L., Li, L., Heymsfield, G. M., Coon, M., & Emory, A. (2021). The NASA/GSFC 94 GHz airborne solid state cloud radar system (CRS). *Journal of Atmospheric and Oceanic Technology*, *38*(5), 1001–1007. https://doi.org/10.1175/JTECH-D-20-0127.1

Westbrook, C. D., Illingworth, A. J., O'Connor, E. J., & Hogan, R. J. (2010). Doppler lidar measurements of oriented planar ice crystals falling from supercooled and glaciated layer clouds. *Quarterly Journal of the Royal Meteorological Society*, *136*(646), 260–276. https://doi.org/10.1002/qj.528